Soft Matter

Cite this: *Soft Matter*, 2012, **8**, 4795

www.rsc.org/softmatter

PAPER

Structural evolution of cuboidal granular media

Robert F. Shepherd,[a] Jacinta C. Conrad,[c] Tapan Sabuwala,[b] Gustavo G. Gioia[b] and Jennifer A. Lewis*[a]

Received 25th September 2011, Accepted 27th February 2012
DOI: 10.1039/c2sm06829j

Mono- and bi-disperse rectangular cuboidal granules are assembled from colloid-hydrogel suspensions *via* stop-flow lithography and fully submerged in hexadecane. Their packing density and structural evolution are studied as a function of agitation time using micro-computed X-ray tomography. When subjected to periodic agitation, the granule packing density increases logarithmically in time; concomitantly, the nearest-neighbor separation distance between granules decreases. Akin to spherical granular media, the distributions of Voronoi volume for these granule packings can be scaled using a shifted k-gamma probability distribution. This Boltzmann-type distribution maximizes packing entropy, indicating that the statistical mechanics approach to granular fluctuations is valid for non-spherical granular media.

Introduction

Granular media are dissipative materials composed of discrete particles, typically exceeding 10 μm in size. They are ubiquitous in nature, *e.g.*, sandpiles and soil sediments,[1] and technology,[2] *e.g.*, ceramics,[3–5] food, pharmaceutical,[6] and oil recovery processes.[7–11] For example, in ceramics fabrication, micron-sized primary particles are granulated to facilitate their flow and packing into shape-forming dies and molds. Granular media exhibit a range of mechanical properties that depends upon the configuration or arrangement of individual granules within the system. For example, static packings[12] exhibit yield stresses that when exceeded cause granules to flow and rearrange.[13,14] The density of granule packs typically increases upon external agitation; however, the observed rate of densification may be slow or rapid, depending on the number of available granule configurations during rearrangement.[15–20]

One route for quantitatively relating the structure to the mechanical properties of granular media is the statistical mechanics approach of Edwards.[21,22] For compact granular media exhibiting solid-like behavior, this approach posits that the time average of a system in response to an external driving force coincides with ensemble averages over solid-like states[18] that are thought to be "jammed", *i.e.*, those that are amorphous and exhibit a yield stress.[23–25] Building on this approach, Aste and co-workers[26–28] expressed the entropy as a function of the probability distribution of the Voronoi volume V associated each granule *via* the k-gamma distribution. Specifically, the k-gamma distribution is the probability distribution that maximizes entropy and is a function of a shape parameter, $k = (\bar{V} - V_{min})^2/\sigma^2$, where σ^2 is the variance of V, V_{min} is the minimum possible Voronoi volume for a given granule shape, and $\bar{V}$ is the average Voronoi volume across all granules. Empirical fits to gamma distributions have been reported for a wide variety of amorphous systems that exhibit yield stresses.[29–35] Experiments and computations on granular packs composed of monodisperse spherical granules confirmed that the k-gamma distribution correctly describes the geometric fluctuations during slow compaction.[27] Moreover, the k parameter remains nearly constant during compaction, suggesting that the structure of the packing remains amorphous[36] even as its density slowly increases.[27] However, this statistical mechanics approach for spherical granules has yet to be tested for non-spherical granular media.

Unlike the idealized spherical granules studied in experiments and simulation, real granular media generally exhibit a range of sizes and shapes. Scant attention has been given to nonspherical or polydisperse granules, whose maximal packing fractions[37,38] exceed the close-packing limit of monodisperse spheres.[39,40] Empirical studies of these granular systems are hindered by the lack of available granular media of controlled shape and size. To date, the packing density of gaming dice[38] and M&Ms[37] as well as the compaction dynamics of polydisperse rice grains[18] and toy plastic cubes[41,42] have been studied. While these opportunistic systems provide a first glimpse into the relationship between granule shape and packing behavior, their shape, size dispersity, and surface roughness cannot be specifically tailored. Recent advances in top-down fabrication techniques, such as particle replication in non-wetting templates (PRINT[43]) and photolithography,[44,45] enable the production of nonspherical particles of arbitrary two-dimensional shape. However, these particles have yet to be explored as model granular media. Moreover, these techniques do not easily permit control over surface roughness, a critical factor in mediating granular interactions.[46]

[a]*Frederick Seitz Materials Research Laboratory, Materials Science and Engineering Department, University of Illinois, Urbana, Illinois 61801. E-mail: jalewis@illinois.edu*
[b]*Mechanical Science and Engineering, University of Illinois, Urbana, Illinois 61801*
[c]*Department of Chemical and Biomolecular Engineering, University of Houston, Houston, Texas 77204*

Here, we demonstrate a new route for fabricating non-spherical granular media of controlled shape and size *via* stop-flow lithography.[47] Specifically, monodisperse cuboidal (MC) and brick-shaped (MB) granules and bidisperse cuboidal blends (BC) are produced. The density, pair correlation function, and density fluctuations in fully submerged granular (MC, MB, and BC) packings are determined as a function of agitation time by X-ray micro-computed tomography (μCT)[48] coupled with image analysis. We find that their packing density increases logarithmically with agitation time, while the nearest-neighbor separation distance between granules decreases slightly. Akin to spherical granules, their Voronoi volume distributions follow the scaling form predicted by the *k*-gamma model despite significant differences in edge convexity, shape, and size. Together, our observations suggest that the granule shape may play only a minimal role in determining packing dynamics in fully submerged granular media.

Experimental methods

Cuboidal granule assembly

Granules with controlled shape and size dispersity are created from a photocurable colloid-hydrogel suspension *via* stop-flow lithography (Figure S1).[47,49] Granules with characteristic sizes on the order of 100 μm are produced at a frequency of roughly 100 Hz. These granules are composed of silica microspheres of diameter 500 ± 25nm with a colloid volume fraction $\phi_{SiO2} \approx 0.64$; individual microspheres on the granule surface can be resolved using atomic force microscopy (AFM; Fig. S1). The root-mean square surface roughness of these granules, which is controlled by the microsphere radius, is 150 nm. After photopolymerization, the granules are extracted from suspension and cleaned by washing them in acetone and heptane. To reduce attractive interactions, the granules are immersed in hexadecane, which lowers the Hamaker constant, A_H, from $A_H = 6.3 \times 10^{-20}$ J (silica in air) to $A_H = 0.3 \times 10^{-20}$ J (silica in hexane).[50]

To assemble fully submersed granular packings, we gently add the nonspherical granules to X-ray transparent, polyimide tubes of internal diameter ≈ 2.0 mm filled with hexadecane (Figure S2). The tip of a pipette containing granules immersed in hexadecane is brought into contact with the meniscus present within the hexadecane-filled tube. When the pipette is inverted, the granules gently fall to the bottom of the tube to form a loosely packed structure. To eliminate the static electricity that is built up during handling, the granule packs are subjected to an antistatic gun (Zerostat). To investigate their structural evolution, we agitated the samples by repeated horizontal shaking for times ranging from 0 to 25×10^3 s with a period of 2 s and a maximum velocity of 2 cm s^{-1}. We restricted our experiments to this relatively slow oscillation (as compared to typical oscillation frequencies of 4 Hz in other horizontal-shaking experiments performed on spherical granules[51]), because higher frequencies and amplitudes completely disrupted the granular pack and dispersed the granules throughout the fluid volume. Under these conditions, we did not observe any crystallization in our experiments, unlike prior observations on horizontally oscillated spherical granules.[51,52] The relative acceleration in our system is $\Gamma = A\omega^2/g \approx 2 \times 10^{-4}$, calculated using an amplitude $A \approx 0.67$ cm and a frequency $\omega = 0.5$ Hz, well below the threshold for relative acceleration $\Gamma = 0.4$ typically needed for crystallization of spheres.[52]

Force calculations

We estimated the minimum and maximum adhesion forces between granules due to van der Waals (vdW) interactions using the Hamaker constants from Lee.[50] We first estimated the van der Waals force between two spheres[53] as $F_{sph-sph} = -A_H R/12D^2$, where R is the sphere radius and D is the separation between the spheres. For two silica spheres of radius $R = 500$ nm suspended in hexadecane, we estimated a separation distance $D = 0.2$ nm between the spheres, leading to a vdW force $F_{sph-sph} = -6.9 \times 10^{-4}$ nN. To calculate the force of adhesion, we estimated the minimum and maximum number of colloid-colloid contacts for each cuboidal granule. AFM images of the surface of a granule (Figure S1) show that there is approximately one protruding colloid per square micron of surface area, and thus two colloid-colloid contacts for each square micron when two granules are in contact. From the minimum and maximum contact areas for each granule, which are set by the areas of the cuboid faces, we estimated the van der Waals adhesion force F_{vdW} between granules as 1.4–1.7 nN (MC), 1.4–5.2 nN (MB), and 1.4–3.9 nN (BC).

To assess the influence of van der Waals forces on the compaction of granular packs, we also calculated for each granule shape the gravitational force, $F_{grav} = \rho_{avg} Vg$, where V and ρ_{avg} are the volume and average density of a granule, respectively. The packing fraction of silica colloids ($\rho_{SiO2} = 2.25$ g/cc) within the granules is $\phi \approx 0.64$[49] and the interstices ($1 - \phi \approx 0.36$) are assumed to be filled with hexadecane ($\rho_{C16} = 0.75$ g/cc). Hence, the effective density of the granules immersed in hexadecane is $\rho_{avg} = 1.7$ g/cc. From the granule volumes for each cuboid, we estimate that the gravitational force F_{grav} is 1.8 nN (MC), 5.3 nN (MB), and 2.9 nN (BC), respectively.

Three-dimensional imaging of cuboidal granular packs

We imaged the fully submerged granular media in three dimensions using X-ray micro-computed tomography (μCT) (MicroCT-200, X-Radia, Pleasanton, CA). To minimize wall effects, the granular packings are imaged at a minimum distance of four cuboidal granule edge lengths from the interior surface of tubes. For each sample, we imaged 500 to 1200 granules at a magnification of 10× or 20× and resolutions of 0.93 μm/pixel or 1.63 μm/pixel, respectively. This resolution is sufficient to allow individual granules within the packed bed to be clearly visualized, because their X-ray scattering cross-section is much larger than that of hexadecane.

Imaging analysis

The granular packings are digitally reconstructed using Imaris visualization software (Bitplane Software, Zurich, Switzerland). From these images, we determined the granule volume fraction ϕ, the pair distribution function $g(r)$, the distribution of Voronoi volume V, and the *k*-gamma distribution as a function of agitation time. To calculate granule volume fraction ϕ, we measured the volume of granules and hexadecane-filled voids by

thresholding the pixel intensity using an ImageJ plugin that implements Otsu's thresholding algorithm.[54] We estimate that this threshold procedure combined with the high contrast in intensity between hexadecane and silica leads to an error of no more than one pixel at the edge of each granule. For the granules studied here, the length of the shortest side in a μCT image is 25 pixels, leading to a maximum error in the absolute volume fraction of no more than 12% (as estimated for a cuboid granule).

To locate the positions of all granules within each three-dimensional image stack, we first segmented the granules to separate touching neighbors and thereby assigned a unique identity to each granule. We then extracted the centroids of each granule from the segmented granule matrix. The pair-correlation distribution function $g(r)$ is calculated from the positions of the centroids as a function of the time of agitation using standard algorithms in IDL (ITTVIS, Boulder CO).

To assess the local structure of the granule packings, we calculated the Voronoi volume, defined as the volume in space closest to each granule. Because our cuboidal granules have flat faces, we cannot simply apply the standard algorithms developed for calculating the Voronoi volume of spheres. Instead, we calculated the Voronoi volume, V, for each granule in the packed bed from the μCT images, using a method similar to that reported by Al-Raoush and Alshibli.[55] We used the surfaces of the segmented granules as a starting location to determine each individual granule's Voronoi volume. For each granule, we calculated a Euclidean distance map from its surface to the next nearest surface, and subtracted this map from its Euclidean distance map calculated in the absence of other granules. This difference is the volume of unoccupied space closest to each granule. We finally calculated the Voronoi volume for each granule by summing the granule volume and the volume of unoccupied space closest to it.

The k-gamma distribution is the probability density function (PDF) to find a packing of k cells that occupy a Voronoi volume V in an experiment where the average Voronoi volume of an occupied cell is $\bar{V}$.[27] This PDF maximizes the functional entropy[26–28] and is given by

$$f(V,k) = \frac{k^k (V - V_{\min})^{k-1}}{\Gamma(k)(\overline{V} - V_{\min})^k} \exp\left(-k \frac{V - V_{\min}}{\overline{V} - V_{\min}} \right) \qquad (1)$$

where $V_{\min}$ is the minimum Voronoi volume per granule, and $k = (\bar{V} - V_{\min})^2/\sigma^2$, where σ^2 is the variance of V.[27] The parameter k thus quantifies the shape of the distribution, and $\bar{V} - V_{\min}$ quantifies its scale.[56]

To fit our experimental data to this distribution function, we first labeled all granules with a unique identification number. The accuracy of the nonlinear fitting to the stretched Boltzmann-like form of the k-gamma distribution (eqn (1)) is highly sensitive to the minimum Voronoi value, $V_{\min}$. We found that poor statistics in the long tails of the Voronoi volume distribution lead to large differences in the shape and scale parameters. We therefore estimated the probability density function (PDF) of Voronoi volumes $P(V)$ from the experimentally measured distribution using the kernel density estimator ksdensity.m as implemented in Matlab (MathWorks, Natick MA); $P(V)$ is evaluated at 36 equally spaced points using a Gaussian kernel centered at each point. We then used nonlinear least squares regression to fit the PDF to the analytical function proposed by Aste, taking $\bar{V}$ and k as fit parameters. Finally, we estimated the variance of the distribution from the analytical fit parameters as $\sigma^2 = (\bar{V} - V_{\min})^2/k$. The fit values for $\bar{V}$, σ^2, and k are reported in Supplementary Information (Table S1).

Results and discussion

To demonstrate the utility of our microfluidic granulation method for investigating fundamental problems in granular physics, we created three types of granular media composed of different shapes and sizes (Fig. 1). Monodisperse cuboidal (MC) granules have dimensions of $50 \times 50 \times 40$ μm^3 with a coefficient of variation c.v. <12% (Fig. 1a). Monodisperse brick-shaped granules (MB) have dimensions of $150 \times 50 \times 40$ μm^3, yielding a maximum aspect ratio of 3.75, and a c.v. < 10% (Fig. 1b). Bidisperse cuboidal granules (BC), with respective dimensions of $50 \times 50 \times 40$ μm^3 (c.v. < 10%) and $75 \times 75 \times 40$ μm^3 (c.v. < 10%), are blended in a 1 : 20 number ratio of small-to-large cuboids (Fig. 1c). Using the radii of spheres with equivalent volumes to the small and large cuboids, we estimate the polydispersity of the BC media to be $\delta \approx 0.13$. This minimal set of building blocks allows us to test the effects of both shape and size dispersity on the packing behavior and structural evolution of fully submerged granular media during agitation.

We characterize the structure of the resulting granular packings in three dimensions using μCT. This technique allows large sample volumes to be imaged with submicron resolution, thereby enabling the locations of the centroids of individual cuboidal granules to be determined as shown in Fig. 2(a). From this data, we calculate the bulk density of granule packings as well as metrics of their local structure, including the pair-correlation function, Voronoi volume, and k-gamma distribution. As one example, the interfaces between neighboring Voronoi volumes, denoted by the red surfaces, are shown in Fig. 2(b)—(d).

We first determined the kinetics of bulk compaction by imaging fully submerged granule packings at regular time intervals during agitation. The initial volume fraction occupied by these packings depends on both granular shape and size dispersity, as shown in Fig. 3. We find average values of $\phi_{MC} = 0.47 \pm 0.15$, $\phi_{MB} = 0.38$, and $\phi_{BC} = 0.33$ for MC, MB, and BC samples, respectively. Both the brick (MB) and bidisperse (BC) granular packings exhibit lower initial densities than those containing monodisperse cuboids. Their lower initial volume fractions reflect structural frustration that arises from the large aspect ratio of the MB granules and the size dispersity between the two types of BC granules, respectively. Remarkably, the bidisperse granular media has the lowest initial density, even though increasing size dispersity often leads to more dense maximal packings.[57] The MC granule packings undergo steady densification as a function of agitation, with the volume fraction increasing logarithmically in time. This behavior has been observed for spherical granule packings.[16] For the data collected, we are unable to distinguish between corrected functional forms suggested for the time dependence of the density,[58–62] such as an inverse-logarithm[16] or a stretched exponential.[19] The rate of compaction $\tau = d\phi/d\log t$ of the MC sample, calculated from the slope of the density as a function of time (Table 1), is constant over all agitation times. By contrast, the MB and BC packings

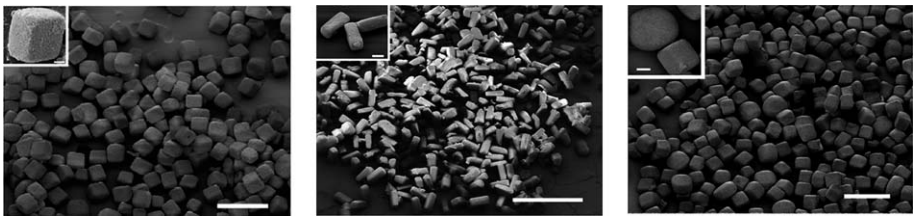

Fig. 1 Scanning electron micrographs of cuboidal granular media used in this study. (a) Monodisperse cuboidal (MC) granules [scalebar 150 μm]; inset: a cuboidal granule [scalebar 10 μm]. (b) Monodisperse brick-shaped (MB) granules [scalebar 500 μm]; inset: three brick-shaped granules [scalebar 50 μm]. (c) Bidisperse cuboidal (BC) granules [scalebar 150 μm]; inset: two cuboidal granules [scalebar 10 μm].

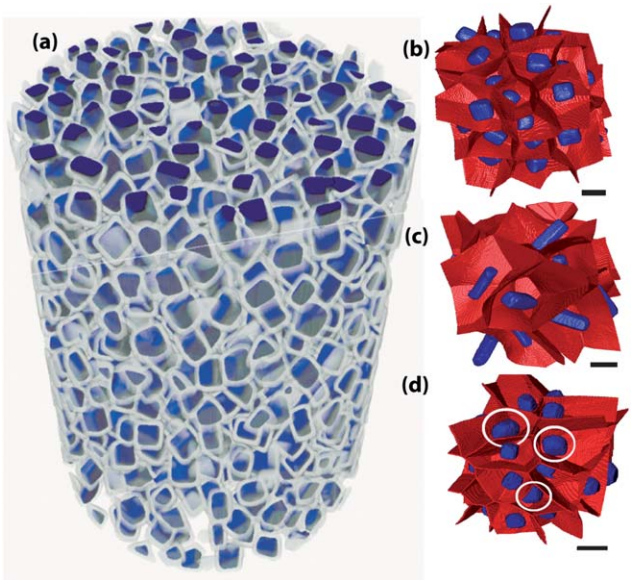

Fig. 2 (a) Representative 3D reconstruction of a cuboid granule pack, where each granule (blue) surface has been eroded (gray) to facilitate segmentation. (b—d) Outlines of the Voronoi volumes (red) for a subset of granules (shown in blue) in (b) MC, (c) MB, and (d) BC granule packings, respectively. Scalebars are 100 μm, 50 μm, 50 μm, and 70 μm, respectively.

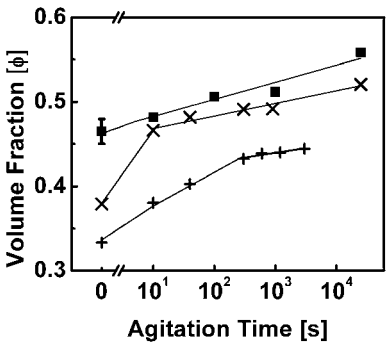

Fig. 3 Log-linear plot of the volume fraction *versus* agitation time for MC (■), MB (×), and BC (+) granule packings. The solid lines indicate logarithmic fits to the experimental data. Each data point represents a single run, except for the initial point for the MC sample in which three replicate experiments were performed.

exhibit two distinct regimes of logarithmic compaction, with a fast initial compaction rate followed by a slower compaction rate. These compaction rates differ by about an order of magnitude. For the MB packings, the duration of the fast compaction is very short, indicating that even small changes in the local structure can induce large changes in the bulk volume. Indeed, these structures are very fragile and can collapse even upon slight agitation. For the BC packing, the duration of fast compaction is much longer than in the MB packing, and the subsequent slow compaction is slightly slower than that of either the MC or MB packings. We surmise that this slower rate is due to the fact that the smaller cuboids are too large to fit into the interstices between the larger cuboids. Our findings suggest that both shape and size dispersity determine the rate of compaction of nonspherical granular media.

The theoretical maximum packing fraction of MC and MB granules is unity. However, at agitation times in excess of 10^4 s, these granular packs are still far from their maximal packing fraction. Clearly, much longer agitation times are needed to approach maximal packing densities for these systems. To explain this surprising result, we compare the relative strengths of the gravitational and van der Waals (vdW) forces that act upon the granules. We estimated that that the maximum magnitudes of the vdW forces F_{vdW} are 1.7 nN and 5.2 nN for MC and MB granules, respectively. These attractive forces are similar in magnitude to the gravitational force, F_{grav}, that drives compaction, 1.8 nN and 5.3 nN for MC and MB, respectively. By contrast, for spherical glass granules (1 mm diameter), a common choice for studies of granular structure and compaction,[63] the magnitude of the gravitational force $F_{grav} = 12$ μN is an order of magnitude larger than that of the van der Waals force $F_{VdW} = 1.3$ μN. Compared to mm-scale glass beads in which gravitational forces dominate compaction, the nearly equal magnitudes of van der Waals and gravitational forces for these cubiodal granules suggest that they should approach their maximum packing fractions far more slowly.

The increase in bulk density as a function of agitation time indicates that the fully submerged granule packings undergo structural changes at the local scale during compaction. To probe the evolution of local structure, we first measure the pair-correlation function $g(r)$ for the MC and BC packings; the number of individual granules imaged within the MB packing was too small to obtain reasonable statistics. For the MC packing, the position of the first maximum in the pair correlation function shifts to smaller values of r/a as the agitation time increases, indicating that the nearest-neighbor separation significantly decreases during agitation (Fig. 4a). A similar shift is also seen in the position of the weak second maximum for the MC sample. These shifts in position occur without changes in the widths of the maxima, indicating that the sample slowly evolves toward a more

compact structure without significant translational ordering. By contrast, neither the position nor the width of the first maximum of $g(r)$ of the BC packing, which contains a bimodal distribution of cuboid sizes, changes with increasing agitation time within measurement error (Fig. 4b). Hence, the large changes in initial volume fraction observed for the BC packing likely arise due to slight local reorientation and alignment of the granules. More sensitive measurements of the local orientation of individual granules[38] are required to fully elucidate the observed differences in granule packs of varying shape and size distribution.

To further probe their local structure evolution, we measured the distribution of Voronoi volume for each sample as a function of agitation time. Representative distributions of Voronoi volume are shown for the MC, MB, and BC packings as a function of agitation time are shown in Fig. 5. From the experimentally measured distributions (symbols), we calculated the experimental probability distribution functions (PDF) for the Voronoi volume using the kernel density estimation (lines) and fit each PDF to the analytical function proposed by Aste *et al.* (eqn (1)).

The agitation-enhanced compaction is captured by the distributions of Voronoi volume, shown in Fig. 5. The mean and variance of the Voronoi volume distribution for the MC pack both decrease with increasing agitation time. Over 25,000 s of agitation, the mean Voronoi volume decreases by roughly 12% (from $\bar{V} = 6.5 \times 10^2\ \mu m^3$ to $\bar{V} = 5.7 \times 10^2\ \mu m^3$) and the variance decreases by roughly 18% (from $\sigma^2 = 7.9 \times 10^3\ \mu m^6$ to $\sigma^2 = 6.5 \times 10^3\ \mu m^6$, Table S1), confirming that the structure becomes more homogeneous with increasing agitation. Similarly, the mean and variance of the Voronoi volume distribution for the MB packing decreased by 9% and 15%, respectively (from $\bar{V} = 9.4 \times 10^2\ \mu m^3$ to $\bar{V} = 8.6 \times 10^2\ \mu m^3$ and $\sigma^2 = 30.9 \times 10^3\ \mu m^6$ to $\sigma^2 = 26.4 \times 10^3\ \mu m^6$, Table S1). The relatively small changes in the Voronoi volume distribution are consistent with our hypothesis that the large changes in bulk structure for the MB packing arise from local reorientations of the granules. The magnitude of the changes in Voronoi volume over time are broadly consistent with prior results on spherical granules,[26–28] confirming that granular shape does not strongly affect the rate of compaction.

Unlike monodisperse granule (MC and MB) packings, bidisperse cuboidal granule packs (BC) exhibit more pronounced structural changes as a function of agitation time. Both the initial mean ($\bar{V} = 3.6 \times 10^3\ \mu m^3$) and variance ($\sigma^2 = 6.7 \times 10^5\ \mu m^6$) of

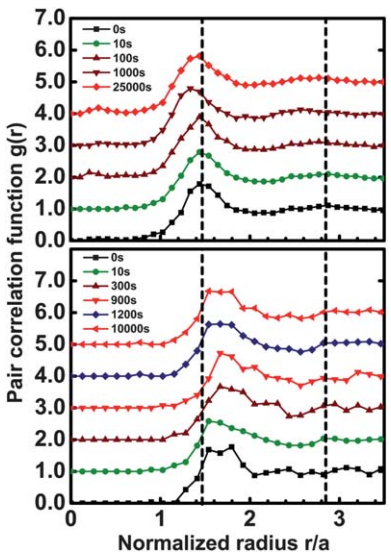

Fig. 4 Pair-correlation function $g(r)$ *versus* the normalized separation distance r/a for (a) MC and (b) BC granule packings, where $a = 40$ μm, the minimum side length for all granules. The vertical dotted lines indicate the initial positions of the first and second maxima for the MC sample. Curves are offset by unit increments in the vertical direction to improve clarity.

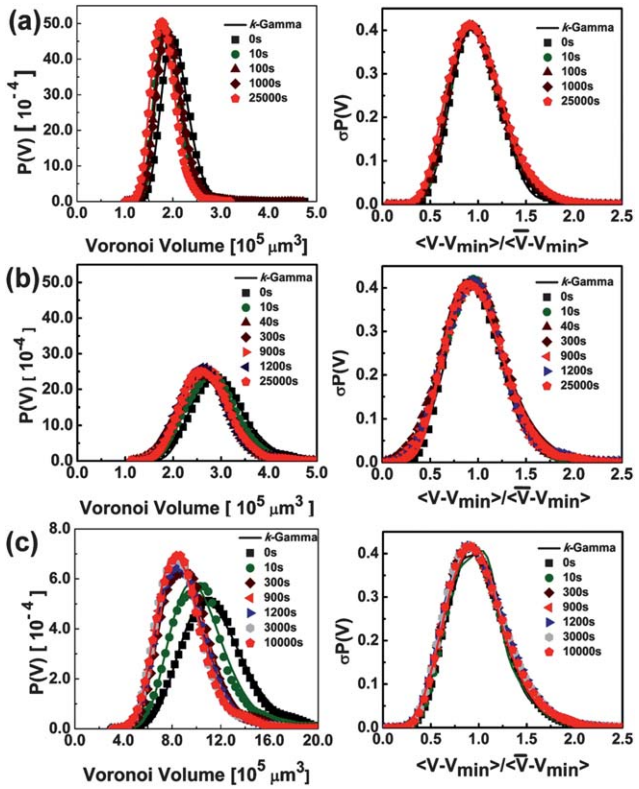

Fig. 5 Probability density function (PDF) (left) and scaled PDF (right) of the Voronoi volume distributions for (a) MC, (b) MB, and (c) BC granule packings. Symbols indicate different agitation times; lines indicate fits to the functional form in eqn (1).

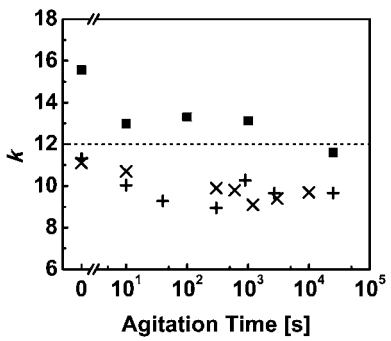

Fig. 6 Values of the shape parameter k obtained from fitting the k-gamma distribution to the Voronoi volume distributions for MC (■), MB (×) and (BC) (+) granule packings. The dashed line indicates the value expected for mechanically stable packings of spherical granules.

the Voronoi volume distribution are larger than the corresponding values measured for the other systems, even though the volumes of the two granules in the BC packing are smaller than those in the MB packing. This surprising result stems from the low bulk density measured for the BC packing, shown in Fig. 1, and likely arises because the small cuboidal granules cannot fit within the interstices present between the larger cuboidal granules. After the BC packing is agitated for 10,000 s, the mean and variance dramatically decrease by 23% and 46%, respectively (Fig. 5c and Table S1), indicating that agitation can overcome this structural frustration.

Remarkably, despite the clear differences in compaction behavior, all three systems can be well fit to the *k*-gamma distribution,[27] as shown by the solid lines in Fig. 5 (left). Furthermore, by rescaling the volume (*x*-axis) as $(V - V_{\min})/(\bar{V} - V_{\min})$ and the distribution of Voronoi volumes (*y*-axis) as $\sigma P(V)$, all of the distributions collapse onto a single master curve, as shown in the right side of Fig. 5. The good collapse of all of these data indicates that the jamming conditions are phenomenologically similar throughout agitation, despite the clear increase in packing fraction (Fig. 2) and slight change in nearest-neighbor distance (Fig. 3). From the fits to the *k*-gamma distribution, we extracted the shape (k) and scale ($\bar{V} - V_{\min}$) parameters (Table S1). We find that the k parameter, which is analogous to the specific heat in thermal systems,[27] is relatively constant as a function of the agitation time for all three types of cuboidal granules studied. Moreover, most k values lie within the range from 9–13 as shown in Fig. 6, very similar to the value of $k \sim 12$ reported for mechanically stable, amorphous packings of spherical granules.[27] The k values of both the monodisperse and bidisperse cuboidal granules are similar to those expected for spheres at all agitation times, in contrast to the large difference in the shape parameter reported for monodisperse ($k \approx 14$) and polydisperse ($k \approx 2$) attractive emulsions.[31] The near-constant values of k indicate that each of these nonspherical packings corresponds to a mechanically stable state[23,24,27] and that these states appear repeatedly as the system evolves from one local minimum to another during the densification process.

Conclusions

We have demonstrated a new approach to fabricating granules of controlled shape and size dispersion for exploring fundamental problems in granular physics. Using stop-flow lithography, both cuboid and brick-shaped granules were produced and assembled into fully submerged granular packings of varying shape and size dispersity. By creating granular media composed of micro-sized primary particles, we have investigated a system in which both attractive van der Waals forces and gravitational forces play an important role in their packing behavior and structural evolution. We have shown that their packing density increases logarithmically with agitation time, and, concomitantly, the nearest-neighbor separation distance between granules decreases slightly. The relative strength of the attractive and gravitational forces acting on these granules suppresses densification; hence, long periods of agitation are required to approach their maximal packing densities. Our observations suggest that the statistical mechanics approach of Edwards[22] may be useful in describing the behavior and compaction dynamics of fully submerged[64] nonspherical and polydisperse[57] granular systems, Our three-dimensional data acquired by micro-computed tomography will enable further studies of the structure of these systems; for example, analysis of the local structural anisotropy through Voronoi polyhedra.[65] Finally, using this method, granules composed of different sized colloids can be fabricated to investigate the effects of surface roughness on granular packings in natural and technological systems.

Acknowledgements

This work is based on research supported by the National Science Foundation (Grant#: DMR-0652424). The authors gratefully acknowledge the valuable contributions of P. S. Doyle (MIT), who shared his expertise of stop-flow lithography with our group.

References

1 R. A. Bagnold, *Proc. R. Soc. London, Ser. A*, 1966, **295**, 219–232.
2 P. J. Sherrington, *Granulation*, Heyden, London; Philadelphia, 1981.
3 T. A. Deis and J. J. Lannutti, *J. Am. Ceram. Soc.*, 1998, **81**, 1237–1247.
4 S. J. Lukasiewicz, *J. Am. Ceram. Soc.*, 1989, **72**, 617–624.
5 R. A. Youshaw and J. W. Halloran, *Ceram. Bull.*, 1982, **61**, 227–230.
6 K. Masters, *Spray Drying Handbook*, 4th edn, Wiley, New York, 1985.
7 L. P. Kadanoff, *Rev. Mod. Phys.*, 1999, **71**, 435–444.
8 H. M. Jaeger, S. R. Nagel and R. P. Behringer, *Rev. Mod. Phys.*, 1996, **68**, 1259–1273.
9 M. Buchanan, *Nature*, 2003, **425**, 556–557.
10 K. Chen, J. Cole, C. Conger, J. Draskovic, M. Lohr, K. Klein, T. Scheidemantel and P. Schiffer, *Nature*, 2006, **442**, 257.
11 H. M. Jaeger and S. R. Nagel, *Science*, 1992, **255**, 1523–1531.
12 R. M. Nedderman, *Statics and Kinematics of Granular Materials*, Cambridge Univ. Press, Cambridge, 1992.
13 G. Gioia, S. E. Ott-Monsivais and K. M. Hill, *Phys. Rev. Lett.*, 2006, **96**, 138001.
14 P. Jop, Y. Forterre and O. Pouliquen, *Nature*, 2006, **441**, 727–730.
15 M. P. Ciamarra, M. Nicodemi and A. Coniglio, *Phys. Rev. E: Stat., Nonlinear, Soft Matter Phys.*, 2007, **75**, 021303.
16 J. B. Knight, C. G. Fandrich, C. N. Lau, H. M. Jaeger and S. R. Nagel, *Phys. Rev. E: Stat. Phys., Plasmas, Fluids, Relat. Interdiscip. Top.*, 1995, **51**, 3957–3963.
17 E. R. Nowak, J. B. Knight, E. Ben-Naim, H. M. Jaeger and S. R. Nagel, *Phys. Rev. E: Stat. Phys., Plasmas, Fluids, Relat. Interdiscip. Top.*, 1998, **57**, 1971–1982.
18 P. Ribiere, P. Richard, D. Bideau and R. Delannay, *Eur. Phys. J. E*, 2005, **16**, 415–420.
19 P. Philippe and D. Bideau, *Europhys. Lett.*, 2002, **60**, 677–683.
20 T. Boutreux and P. G. de Gennes, *Physica. A*, 1997, **244**, 59–67.
21 A. Mehta and S. F. Edwards, *Physica. A*, 1989, **157**, 1091–1100.
22 S. F. Edwards and C. C. Mounfield, *Physica. A*, 1996, **226**, 1–11.
23 A. J. Liu and S. R. Nagel, *Nature*, 1998, **396**, 21–22.
24 M. E. Cates, M. D. Haw and C. B. Holmes, *J. Phys.: Condens. Matter*, 2005, **17**, S2517–S2531.
25 C. S. O'Hern, S. A. Langer, A. J. Liu and S. R. Nagel, *Phys. Rev. Lett.*, 2001, **86**, 111–114.
26 T. Aste, *J. Phys.: Condens. Matter*, 2005, **17**, S2361–S2390.
27 T. Aste and T. Di Matteo, *Phys. Rev. E: Stat., Nonlinear, Soft Matter Phys.*, 2008, **77**, 021309.
28 T. Aste, M. Saadatfar and T. J. Senden, *Phys. Rev. E: Stat., Nonlinear, Soft Matter Phys.*, 2005, **71**, 061302.
29 D. Weaire, J. P. Kermode and J. Wejchert, *Philos. Mag. B*, 1986, **53**, L101–L105.
30 E. Pineda, P. Bruna and D. Crespo, *Philos. Mag.*, 2004, **84**, 2023–2039.
31 I. Jorjadze, L. Pontani, K. A. Newhall and J. Brujic, *Proc. Natl. Acad. Sci. U. S. A.*, 2011, **108**, 4286–4291.
32 E. Sultan and A. Boudaoud, *Phys. Rev. Lett.*, 2006, **96**, 136103.
33 F. W. Starr, S. Sastry, J. F. Douglas and S. C. Glotzer, *Phys. Rev. Lett.*, 2002, **89**, 125501-125501–125501-125504.

34 J. C. Conrad, F. W. Starr and D. A. Weitz, *J. Phys. Chem. B*, 2005, **109**, 21235–21240.
35 P. Varadan and M. J. Solomon, *Langmuir*, 2003, **19**, 509–512.
36 G. D'Anna and G. Germaud, *Nature*, 2001, **413**, 407–409.
37 A. Donev, I. Cisse, D. Sachs, E. Variano, F. H. Stillinger, R. Connelly, S. Torquato and P. M. Chaikin, *Science*, 2004, **303**, 185501.
38 A. Jaoshvili, A. Esakia, M. Porrati and P. Chaikin, *Phys. Rev. Lett.*, 2010, **104**, 4.
39 A. Rosato, K. J. Strandburg, F. Prinz and R. H. Swendsen, *Phys. Rev. Lett.*, 1987, **58**, 1038–1040.
40 F. Ludewig and N. Vandewalle, *Eur. Phys. J. E*, 2005, **18**, 367–372.
41 F. Y. Fraige, P. A. Langston and G. Z. Chen, *Powder Technol.*, 2008, **186**, 224–240.
42 J. Baker and A. Kudrolli, *Phys. Rev. E: Stat., Nonlinear, Soft Matter Phys.*, 2010, **82**, 061304.
43 E. Brown, N. A. Forman, C. S. Orellana, H. J. Zhang, B. W. Maynor, D. E. Betts, J. M. DeSimone and H. M. Jaeger, *Nat. Mater*, 2010, **9**, 220–224.
44 S. Badaire, C. Cottin-Bizonne, J. W. Woody, A. Yang and A. D. Stroock, *J. Am. Chem. Soc.*, 2007, **129**, 40–41.
45 C. J. Hernandez and T. G. Mason, *J. Phys. Chem. C*, 2007, **111**, 4477–4480.
46 J. R. Royer, D. J. Evans, L. Oyarte, Q. Guo, E. Kapit, M. E. Mobius, S. R. Waitukaitis and H. M. Jaeger, *Nature*, 2009, **459**, 1110–1113.
47 R. F. Shepherd, P. Panda, Z. Bao, K. H. Sandhage, T. A. Hatton, J. A. Lewis and P. S. Doyle, *Adv. Mater.*, 2008, **20**, 4734–4739.
48 E. L. Ritman, *Annu. Rev. Biomed. Eng.*, 2004, **6**, 185–208.
49 R. F. Shepherd, J. C. Conrad, S. K. Rhodes, D. R. Link, M. Marquez, D. A. Weitz and J. A. Lewis, *Langmuir*, 2006, **22**, 8618–8622.
50 I. Lee, *J. Mater. Sci.*, 1995, **30**, 6019–6022.
51 G. Straßburger and I. Rehberg, *Phys. Rev. E: Stat. Phys., Plasmas, Fluids, Relat. Interdiscip. Top.*, 2000, **62**, 2517–2520.
52 O. Pouliquen, M. Nicolas and P. D. Weidman, *Phys. Rev. Lett.*, 1997, **79**, 3640–3643.
53 J. Israelachvili, *Intermolecular and Surface Forces*, 2nd edn, Academic Press, San Diego, 1992.
54 N. Otsu, *IEEE Trans. Syst. Man Cybern.*, 1979, **9**, 62–66.
55 R. Al-Raoush and K. A. Alshibli, *Physica. A*, 2006, **361**, 441–456.
56 R. V. Hogg and A. Craig, *Introduction to Mathematical Statistics*, Macmillan, New York, 1978.
57 R. S. Farr and R. D. Groot, *J. Chem. Phys.*, 2009, **131**, 244104.
58 A. J. Kolan, E. R. Nowak and A. V. Tkachenko, *Phys. Rev. E: Stat. Phys., Plasmas, Fluids, Relat. Interdiscip. Top.*, 1999, **59**, 3094–3099.
59 M. Nicolas, P. Duru and O. Pouliquen, *Eur. Phys. J. E*, 2000, **3**, 309–314.
60 F. X. Villarruel, B. E. Lauderdale, D. M. Mueth and H. M. Jaeger, *Phys. Rev. E: Stat. Phys., Plasmas, Fluids, Relat. Interdiscip. Top.*, 2000, **61**, 6914–6921.
61 A. Castellanos, J. M. Valverde and M. A. S. Quintanilla, *Phys. Rev. Lett.*, 2005, **94**, 075501.
62 P. Richard, M. Nicodemi, R. Delannay, P. Ribiere and D. Bideau, *Nat. Mater.*, 2005, **4**, 121–128.
63 G. Gioia, A. M. Cuitiño, S. Zheng and T. Uribe, *Phys. Rev. Lett.*, 2002, **88**, 204302.
64 J. E. Fiscina, G. Lumay, F. Ludewig and N. Vandewalle, *Phys. Rev. Lett.*, 2010, **105**, 048001.
65 G. E. Schröder-Turk, W. Mickel, M. Schröter, G. W. Delaney, M. Saadatfar, T. J. Senden, K. Mecke and T. Aste, *Europhys. Lett.*, 2010, **90**, 34001.